A COUPLED LATTICE BOLTZMANN - IMMERSED BOUNDARY METHOD TO MODEL THE BEHAVIOUR OF THIN FLEXIBLE STRUCTURES IN FLUIDS

Specklin M.*[1,2], Albadawi A.[1,2], Connolly R.[2], Breen B.[2] and Delaure Y.[1]
[1] School of Mechanical and Manufacturing Engineering,
Dublin City University, Ireland
[2]Sulzer Pump Solutions Ireland Ltd.,
Wexford, Ireland
E-mail: mathieu.specklin2@mail.dcu.ie

ABSTRACT

This article presents a computational model to simulate the fluid interaction with moving flexible thin structures. The model is based on a combination of three numerical approaches, (i) a Lattice-Boltzmann solver for the flow equations, (ii) a finite difference method to solve the solid equation, and (iii) an Immersed Boundary Method (IBM) to model the coupling between the fluid and the solid. The present IBM, based on a direct-forcing approach, preserves the no-slip boundary condition at the interface fluid-solid, and allows using Cartesian uniform lattice encompassing both fluid and solid domains. The flexible solid is modelled as an elastic structure. The resulting governing equation involves thus tension and bending forces as internal forces, the inertial and gravity forces and finally the action of the fluid represented by the IBM forcing.

The method is first validated with reference to an academic test case dealing with numerical simulations of a flapping flag in a free stream. The model shows results in good agreement with the published academic test case. The validation extends to the free motion of rag in a water tunnel and a qualitative comparison is available against experimental data performed with Digital Image Correlation (DIC). Finally, the present method is used to simulate the behaviour of flexible rags in the presence of highly rotating flows at high Reynolds number, as it is the case in stirred tanks.

NOMENCLATURE

f_α	Particle distribution function in the direction α
$\mathbf{c}_\alpha$	Discrete lattice velocity in the direction α
ρ	Density
$\mathbf{u}$	Lattice velocity
$\mathbf{U}_k$	Lagrangian solid velocity
τ	Relaxation time
ω_α	Weight parameters
t	Time
Δt	Discrete lattice time
$\mathbf{x}$	Lattice position
$\mathbf{X}_k$	Lagrangian solid position
$\mathbf{g}$	Body force
$\mathbf{G}$	Gravity force
ε	Slender solid thickness
σ	Tension force
γ	Bending rigidity
ϕ	Tension coefficient
ζ	Bending coefficient

Subscripts & Superscripts

α	Discrete Lattice directions
k	Lagrangian points
i, j	2D Lagrangian frame
s	solid
f	fluid
0	initial
$\prime$	intermediate field
$*$	non dimensional variable
T	Relative to tension
B	Relative to bending

INTRODUCTION

The study of the interactions between fluids and flexible structures is relevant to a broad range of application areas (marine engineering for energy harvesting, biological engineering for heart valves, aeronautics for the strength of flaps in aircraft wings, etc). In the field of waste water pumps, the understanding of the behavior of solid wastes, including rags or fibrous clumps, is of primordial importance. Achieving an optimal hydrodynamic design often requires striking a balance between hydraulic efficiency and anti-clogging performances. One way to reduce the risk of clogging relies on widening the hydraulic passage in the pump, i.e. the gap between the impeller and the volute. This however can rapidly deteriorate the pump efficiency and modify the pump performance characteristics in general. The flexible solids typically found in waste water are of slender structures, and their rate of accumulation is known to depend on the flow conditions, so that the effectiveness of more subtle pump design changes are difficult to assess without accurate computational tools capable of capturing both solid and liquid phases. A complete review of the recent investigations on the mechanism of flapping and bending has been done in [1] for slender 1D filament and 2D planar structures.

From a computational point of view, the Immersed Boundary Method (IBM) appears to be a good candidate for modeling the coupling between fluid and thin flexible structures. The first documented IBM was implemented by Peskin [2] to model the interaction of the blood flow with an heart valve, modeled as a

non-conforming elastic solid. Unlike body-fitted approaches like arbitrary Lagrangian - Eulerian methods [3] for which the background grid adapts to the deforming solid, in the IBM the no-slip condition at the interface fluid-solid is achieved through a momentum forcing. This property allows to handle moving flexible structures on Cartesian grids, simplifying drastically the meshing stage and saving significantly the computational resources. In the case of thin structures, the influence of the solid on the fluid is smeared on the nearby nodes, thanks to Dirac delta functions. The type of momentum forcing is what differentiate one IBM from another.

IBMs have been used with both physical models, Navier-Stokes and Lattice-Boltzmann, to simulate flexible structures in fluids. In the Navier-Stokes context, the problem of a flapping flag has been investigated with IBMs based on penalty [4] or direct forcing [5,6] approaches. Akcabay [7] has used a penalty based IBM to perform washing machine simulation. Similar investigations have been performed with both types of IBM in the Lattice-Boltzmann context. Tian et al. [8] have developed an IBM of a penalty type to study flapping filaments and fish swimming. Favier et al. [9] and De Rosis et al. [10] for their part have considered a direct forcing based IBM. Regarding the dynamic of slender solids, most of the authors derived the governing equation from the variational derivative of the deformation energy. This derivation involves a tension and a bending force for the internal forces. The resulting equation is commonly solved with a Finite Difference Method (FDM) for sake of computational resources, but other types of approach have been used as well for the solid mechanics, as the Finite Element Methods (FEM) in De Rosis et al. [10] for flexible insect wings or a coupled IBM - Material Point Method (MPM) allowing large solid deformation in Gilmanov & Acharya [11].

The model presented in this article has been implemented in the open-source library Palabos. The details for the numerical methods are presented before discussing three simulation cases. The first case is a common benchmark found in the literature and considers a flapping flag in a laminar flow. The next two cases concern the transport and deformation of rags under realistic engineering conditions with turbulent flow. The numerical results obtained are compared against experimental data when available.

NUMERICAL FORMULATION

This section details the numerical procedure adopted for modeling the behavior of thin flexible solids in fluids. Firstly, the fluid equations are presented, according to the Lattice-Boltzmann method. Secondly, the IBM used to account for the presence of the structure in the fluid is defined, and finally the governing equation for the flexible solid is formulated.

The fluid solver: Lattice-Boltzmann modeling

The Lattice-Boltzmann method (LBM) is a discrete model for a fluid composed of particles, whose positions are restricted to specific locations on a lattice grid, and velocities are restricted to a finite set of vectors. In this study, the complete three-dimensional lattice with twenty-seven vectors (D3Q27 model) is used. The latter model, illustrated in Figure 1, has the velocity vectors c_α for $\alpha = 0, ..., 27$. The discrete velocity are listed in Table 1. The evolution of the particle distribution function $f(\mathbf{x},t)$ with the velocity c_α at the lattice node $\mathbf{x}$ and time t reads:

$$f_\alpha(\mathbf{x}+\mathbf{c}_\alpha\Delta t, t+\Delta t) - f_\alpha(\mathbf{x},t) = -\frac{1}{\tau}(f_\alpha(\mathbf{x},t) - f_\alpha^{eq}(\mathbf{x},t)) \quad (1)$$

where Δx is the lattice spacing, Δt is the time step during which the particles travel one lattice spacing, and τ is the relaxation time related to the fluid physical viscosity. The local equilibrium distribution functions f^{eq} are obtained from the Maxwell-Boltzmann equilibrium distribution:

$$f_\alpha^{eq}(\mathbf{x}) = \omega_\alpha \rho[1 + 3\frac{\mathbf{c}_\alpha \cdot \mathbf{u}}{c_s^2} + \frac{9}{2}\frac{(\mathbf{c}_\alpha \cdot \mathbf{u})^2}{c_s^4} - \frac{3}{2}\frac{\mathbf{u}^2}{c_s^2}] \quad (2)$$

where $c_s = 1/\sqrt{3}$ is the discrete speed of sound and ω_α are the weight parameters listed in Table 1. The macroscopic variables ρ and $\mathbf{u}$ of the flow are recovered from the following equations:

$$\rho = \sum_\alpha f_\alpha \quad (3)$$

$$\rho\mathbf{u} = \sum_\alpha f_\alpha \mathbf{c}_\alpha \quad (4)$$

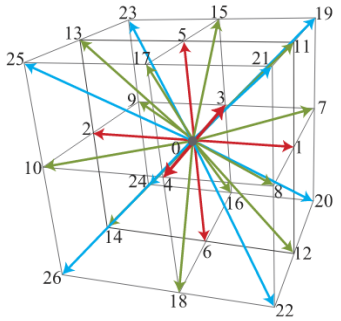

Figure 1. Sketch of the D3Q27 model for a square grid lattice with discrete velocities $\mathbf{c}_\alpha$, where α ranges from 0 to 27.

The Immersed Boundary Method

The IBM employed in this study is based on the Multi Direct Forcing Method (MDFM) proposed by Wang et al. [12] in the Navier-Stokes context. The MDFM has already been coupled to a LBM by Suzuki & Inamuro [13] to study the interaction of fluids with rigid bodies. In this model, the presence of an immersed object in the fluid is accounted through a two-steps approach.

$\mathbf{c}_\alpha$	ω_α
$(0,0,0)$	$8/27(\alpha=0)$
$(\pm1,0,0),(0,\pm1,0),(0,0,\pm1)$	$2/27(\alpha=1,...,6)$
$(\pm1,\pm1,0),(\pm1,0,\pm1),(0,\pm1,\pm1)$	$1/54(\alpha=7,...,18)$
$(\pm1,\pm1,\pm1)$	$1/216(\alpha=19,...,26)$

Table 1. Parameters of the D3Q27 discrete velocity model.

1. A particle distribution function field $f'_\alpha(\mathbf{x},t+\Delta t)$ is evaluated according to equation 1, without taking into account the presence of the solid body.
2. This intermediate field $f'_\alpha(\mathbf{x},t+\Delta t)$ is corrected by the body force accounting for the solid:

$$f_\alpha(\mathbf{x},t+\Delta t) = f'_\alpha(\mathbf{x},t+\Delta t) + 3\Delta x \omega_\alpha \mathbf{c}_\alpha \mathbf{g}(\mathbf{x},t+\Delta t) \quad (5)$$

where $\mathbf{g}$ is the body force representing the action of the solid on the fluid. The body force allows to obtain a no-slip boundary condition at the fluid-solid interface.

In order to evaluate the forcing term, a set of N Lagrangian points $\mathbf{X}_k$ is first considered to define the solid with $\mathbf{U}_k$ the boundary velocity at those points. After the first step of the IBM scheme, an intermediate velocity field $\mathbf{u}'(\mathbf{x},t+\Delta t)$ can be obtained from the field $f'_\alpha(\mathbf{x},t+\Delta t)$ thanks to equations 1 and 4. The Eulerian body force $\mathbf{g}(\mathbf{x},t+\Delta t)$ defined at the lattice node is then determined by the following iterative procedure:

1. At iteration level l, interpolate the Eulerian body force from the values on the nearby Lagrangian surface points.
2. Correct the velocity at the Eulerian nodes with the obtained body force.
3. Interpolate the velocity at the boundary Lagrangian points.
4. Finally, correct the Lagrangian body force at the next iteration with the difference between the fluid and the solid velocities, and go to the next level.

To start the iterative process, the initial value of the Lagrangian body force is obtained by:

$$\mathbf{g}_0(\mathbf{X}_k,t+\Delta t) = \frac{\mathbf{U}_k - \mathbf{u}'(\mathbf{X}_k,t+\Delta t)}{\Delta t} \quad (6)$$

The interpolations from a Lagrangian to an Eulerian variable, and *vice-versa*, are using the standard weighting function proposed by Peskin [2]. It is important to note that only the nearby points are used in the interpolations. A complete description of the algorithm can be found in [13]. The authors have shown that $l=5$ is enough to keep a no-slip condition on the boundary points.

The solid solver

The equation of motion of an elastic slender body is derived in Lagrangian frame (s_i, s_j) using the variational derivative of the deformation energy [14]. The governing equation for a two-dimensional solid, defined by the points $\mathbf{X}_k$ introduced previously, in a 3D flow reads:

$$\Delta\rho \frac{\partial^2 \mathbf{X}}{\partial t^2} = \sum_{i,j=1}^{2} [\frac{\partial}{\partial s_i}(\sigma_{ij}\frac{\partial \mathbf{X}}{\partial s_j}) - \frac{\partial^2}{\partial s_i \partial s_j}(\gamma_{ij}\frac{\partial^2 \mathbf{X}}{\partial s_i \partial s_j})] + \Delta\rho\mathbf{G} - \varepsilon\rho_f \mathbf{g} \quad (7)$$

In Equation 7, $\sigma_{ij} = \phi_{ij}(T_{ij} - T^0_{ij})$ and $\gamma_{ij} = \zeta_{ij}(B_{ij} - B^0_{ij})$, where the terms T_{ij} and B_{ij} denotes for the stretching/shearing effect and the bending/twisting effect respectively. $\mathbf{G}$ is the gravity and $\mathbf{g}$ is the Lagrangian body force introduced in the previous section. The term $\Delta\rho$ denotes the density difference between the filament and the surrounding fluid (which is null for neutrally buoyant objects). This difference comes from Archimedes' law for the gravity term and from the internal mass effect for the inertial term [13]. Finally, the thickness of the solid ε appears in equation 7 from the transformation of the volume integral of the body force to a surface integral over the solid [9].

A first order explicit Finite Difference scheme is used to discretized the motion equation of the slender solid. This type of discretization requires small time step to avoid instability. The resulting linear system is solved with an iterative biconjugate gradient stabilized method (BiCGSTAB). Depending on the case, two different type of boundary condition can be applied (for $i=1,2$):

· a fixed condition with $\mathbf{X} = constant$ and $\frac{\partial^2 \mathbf{X}}{\partial s_i^2} = (0,0)$.

· a free end condition with $\frac{\partial^2 \mathbf{X}}{\partial s_i^2} = (0,0)$, $\frac{\partial^3 \mathbf{X}}{\partial s_i^3} = (0,0)$, $\sigma_{ij} = 0$ and $\gamma_{ij} = 0$.

For comparisons against the numerical benchmarking data, the following non-dimensional parameters can be defined using the flag length L and the free stream velocity $\mathbf{U}_\infty$: the non dimensional time $t^* = tL/\mathbf{U}_\infty$, the non dimensional length $y^* = y/L$, the Reynolds and Froud number $Re = \frac{\rho_f \mathbf{U}_\infty L}{\mu_f}$ and $Fr = gL/{\mathbf{U}_\infty}^2$, the non dimensional tension coefficient and bending rigidity, $\phi^* = \frac{\phi}{\Delta\rho\mathbf{U}_\infty}$ and $\zeta^* = \frac{\zeta}{\Delta\rho{\mathbf{U}_\infty}^2 L^2}$, and finally the non dimensional mass ratio $\rho^* = \frac{\Delta\rho}{\rho_f L}$.

RESULTS AND DISCUSSION

The engineering problems investigated in this study are very demanding in terms of computational resources because of (i) the three dimensional natures of the cases and (ii) the importance of capturing the fluid structure interactions. A refinement limit is quickly reached. Critically coarse grids have been found to be unsuitable for accurate modeling of flow at immersed solid boundaries. For these reasons, performing a grid convergence analysis would require an extremely dense grid and would become quickly impractical. The grids considered in the present work are either based on refinement comparable to those found in the literature or merely limited by computational power. For instance, the 2 second of physical time computed for the transport of a rag considered in Case 2 required more than 17 hours

of calculations on 24 processors.

Case 1: Flapping flag

In the first case, a 2D flag is considered in a 3D flow, according to the set-up of Huang & Sung [15]. The flag shape is square with length L and initial position inclined at an angle 0.1π from the streamwise plane. The size of the computational domain is $[-L,4L]\times[-2L,2L]\times[-L,L]$. Both Eulerian and Lagrangian grids are discretized uniformly with a step size of $L/25$ and $L/50$ respectively. Using a larger domain as in Huang & Sung [15] was found to have a low influence on the flapping mechanism of the flag. The flag is fixed (pinned) from one end and free from the other ends so that the flapping under the effect of the fluid flow will be perpendicular to the flow. The non-dimensional parameters of the problem are listed in Table 2. The time step is chosen the same for the fluid and the solid solvers.

Re	Fr	ρ^*	ϕ^*	ζ^*	Δt^*
200	0	1	100	$1\cdot10^{-4}$	$3\cdot10^{-4}$

Table 2. Non-dimensional parameters for Case 1: flapping flag.

A flapping mechanism similar to the one observed by Huang & Sung [15] is obtained with the current model. Figure 2 shows for instance the vortical structures shedding from the flag. Their hairpin-like geometry is in good agreement with [15]. The time history of the transverse displacement for the mid-point of the flag trailing edge is shown in Figure 3. The flag undergoes sustained oscillations through the IBM coupling. Although the oscillations are consistent with those observed by Huang & Sung [15], two differences can be noticed: (i) a few oscillations are needed to reach a steady periodic flapping, underlying a delay in the flag response, and (ii) the amplitude of the oscillations is slightly overestimated. The different numerical approaches used for the flow solver and the coupling mechanism can be expected to impact the solid response due to the highly dynamic nature of the motion. However the most probable cause for the differences is the value of the tension coefficient which had to be reduced by one order of magnitude in comparison to Huang & Sung [15] because of stability issues in the solid solver.

Case 2: Rag release in a water tunnel

The release of a rag in a water tunnel is considered in this section. DIC tests have been performed to allow solid response characterisation and the experimental data are compared to the numerical results of the present model. The rag is initially clamped with a flagpole system, at the center of the water tunnel. Business paper has been used as a rag material. Approximate values of the rag elastic properties are available in Table 3, along with the numerical parameters of the computation. The flow rate in the water tunnel is about $9.1m^3/h$.

The solid solver is showing an unstable behavior in the neutrally buoyant case, namely when the density difference becomes too small. To overcome this issue, the density difference has been

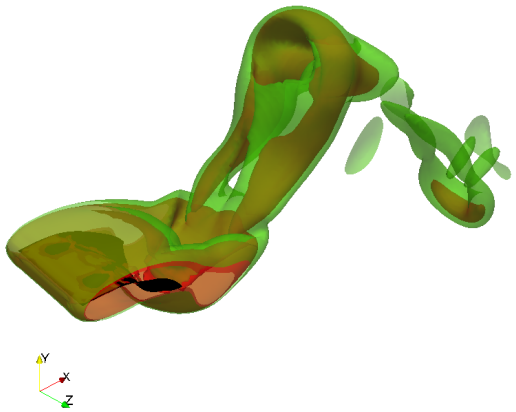

Figure 2. Iso-contours of the vorticity when the flag's trailing edge is near its lowest transverse position. Results obtained with a larger domain (similar to Huang & Sung [15]).

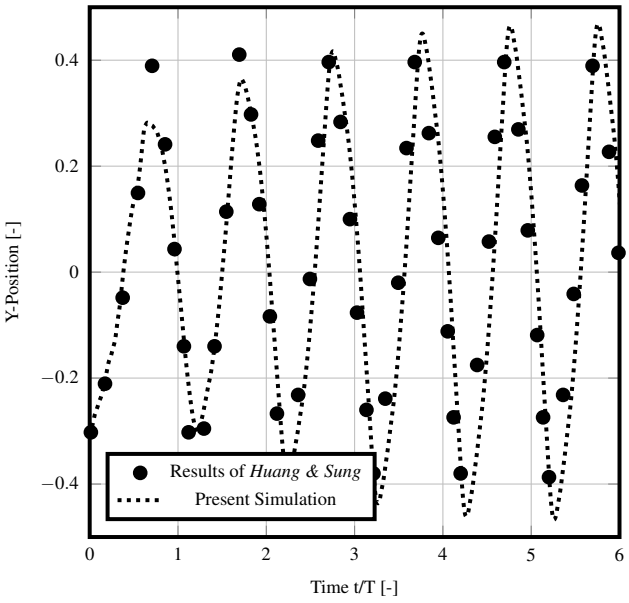

Figure 3. Time evolution of the transverse displacement at the trailing edge center point of the flag.

artificially increased for the inertial term, while it is kept at the physical value for the gravity term. A resolution of $\Delta x = 2mm$ is used for both the fluid and the solid grids. A Smagorinsky based LES (Large Eddy Simulation) model is combined with the fluid solver to model the effect of the subgrid scales in the flow.

Re	Fr	$\Delta\rho$	ϕ	ζ	Δt
21600	2.32	0.03	100	$1\cdot10^{-6}$	$1\cdot10^{-4}$

Table 3. Parameters for Case 2: Rag release.

DIC measurements allow to quantify the displacement of the rag in the three directions of space. Figure 4 shows the experimental data for the transport and the deformation of the rag in the Tunnel at two different times after the release. During the first second, it appears that the rag is not moving much in the stream-

(a) $t = 0.7s$

(b) $t = 1.4s$

Figure 4. Viewing of the transverse displacement of the rag in the water tunnel, obtained by DIC.

wise direction, but it is being pushed upwards by a stream-jet due to the shaft's presence. The jet is visible in Figure 5, which is showing the numerical results obtained with the current model. Similarly, in the numerical simulation the rag is moving upward due to the jet, before settling. One can note as well a similar folding in the transverse direction. Although, the deformation of the rag is comparable, significant differences can be seen between the experimental and the numerical results. The coupled LB-IBM simulates a rag that is moving faster in the streamwise direction and that settle slower than in reality. This difference in the transport can be explained by the artificial increase of inertial term, and needs to be quantify in future works.

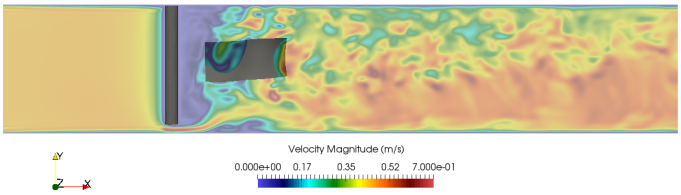

(a) $t = 0.5s$

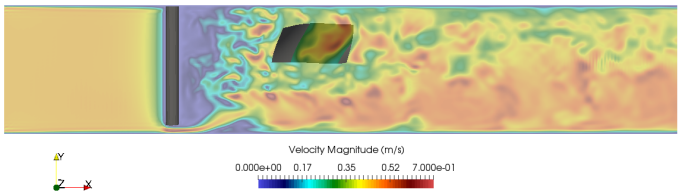

(b) $t = 1.0s$

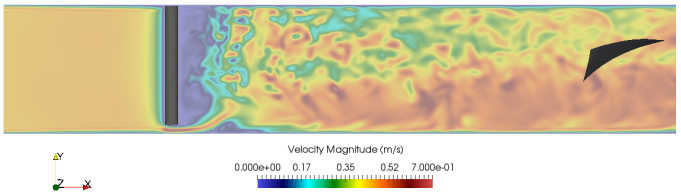

(c) $t = 2.0s$

Figure 5. Snapshots of the rag at different times, with contour of the velocity field in the background.

Case 3: Free motion of rags in mixer

In this last case, the influence of the tension and bending forces on the 2D solid dynamics is investigated. Rags are put in place in a cylindrical mixer of both height and diameter equal to $340mm$. A 4 pitched blade impeller of radius $72mm$ centrally positioned in the tank is driving the mixing with an angular velocity of $15,71rad/s$. The resolution is chosen similar to the Case 2, and Smagorinsky based LES model is used here as well for the turbulence. Two simulations have been performed with different values of the tension and bending coefficients. The numerical and physical parameters for these 2 cases are listed in Table 4.

Case	Re	Fr	$\Delta\rho$	ϕ	ζ	Δt
Sim. 1	5.10^4	0	10	100	$1 \cdot 10^{-6}$	$1 \cdot 10^{-4}$
Sim. 2	5.10^4	0	10	1	$1 \cdot 10^{-8}$	$1 \cdot 10^{-4}$

Table 4. Parameters for Case 3: Rag in mixer. The Reynolds number is calculated using the impeller rotational speed.

The initial conditions for the simulation were based on a fluid at rest with uniform static pressure distribution gravity being neglected. 12.5 impeller revolutions are performed before introducing the rags. Two rags are introduced for each simulation. The first one is centrally positioned $50mm$ below the impeller, while the second one is placed $30mm$ below the tip of one of the blade. The deformation of the rags is illustrated in Figure 6 for both simulation cases. The rags initially below the center of the impeller are slowly sucked by the rotation of the latter. On the contrary the rags placed below the blade's tip are firstly pushed away from the center and toward the bottom, before rising again on the side with the flow. The influence of the elastic force is clearly visible on rags deformation. Low values for the tension and the bending terms allow a more flexible behavior of the rags, which exhibit significant folding in both longitudinal and latitudinal directions.

CONCLUSION

In the present study, an IBM has been presented to model slender flexible solids in fluids. The IBM is coupled to a Lattice-Boltzmann method to solve the fluid governing equations. The model allows for solid deformation thanks to the resolution of a second-order partial differential equation describing the behavior of 2D flexible solids. The solid equation involves the inertial force, the gravity force, the internal forces namely the elastic force, and finally the action of the fluid through the IB forcing term. The overall model has been validated against a standard benchmark for fluid-structure interaction problems and shows a good agreement with results from previous IBM in literature. The model has been secondly applied to engineering cases and promising results were obtained. A high sensitivity to specific parameters has been however highlighted for the solid solver. High tension coefficient for instance, or low density difference, can lead to an unstable behavior of the latter solver. The importance of these parameters needs to be addressed in future works,

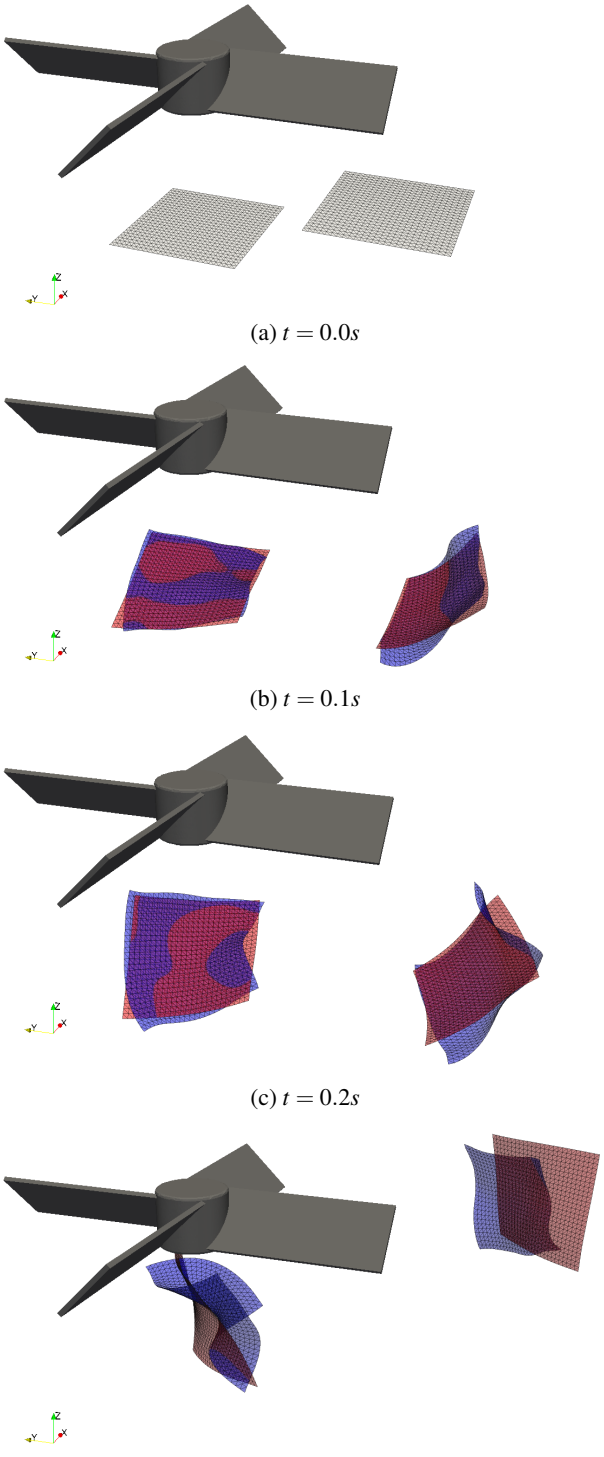

(a) $t = 0.0s$

(b) $t = 0.1s$

(c) $t = 0.2s$

(d) $t = 0.8s$

Figure 6. Snapshots of the rags at different times. The rags in red are computed from Sim. 1 while the rags in blue are obtained from the parameters of Sim. 2.

to perform realistic engineering simulation of rag in a neutrally buoyant context, as it is the case for clogging problems in sewage pumps.

ACKNOWLEDGMENT

The financial support of the Irish Research Council (IRC) under its Employment Based Research Scholarship programme (Grant No. EBPPG/2013/63) is acknowledged. All computations were performed with the machines of the Irish Centre of High-End Computing (ICHEC) and their support is acknowledged.

REFERENCES

[1] Shelly M.J. & Zhang J., Flapping and Bending Bodies Interacting with Fluid Flows, *Annu. Rev. Fluid Mech.*, Vol. 43, 2011, pp. 449-465 .

[2] Peskin C., Flow Patterns Around Heart Valves: A Numerical Method, *Journal of Computational Physics*, Vol. 10, 1972, pp. 252-271.

[3] Donea J., Giuliani S. and Halleux J.P., An arbitrary Lagrangian-Eulerian finite element method for transient dynamic fluid-structure interactions, *Comput. Methods Appl. Mech. Engrg.*, Vol. 33, 1982, pp. 689-723.

[4] Huang W.-X., Chang C.B. and Sung H.J., An improved penalty immersed boundary method for fluid-flexible body interaction, *Journal of Computational Physics*, Vol. 230, 2011, pp. 5061-5079.

[5] Zhu X., He G. and Zhang X., An improved direct-forcing immersed boundary method for fluid-structure interaction simulations, *Journal of Fluids Engineering*, Vol. 136, 2014.

[6] Lee I. & Choi H., A discrete-forcing immersed boundary method for the fluid-structure interaction of an elastic slender body, *Journal of Computational Physics*, Vol. 280, 2015, pp. 529-546 .

[7] Akcabay D.T., Physics Based Washing Machine Simulations, *University of Michigan*, 2007.

[8] Tian F.-B., Luo H., Zhu L., Liao J.C. and Lu X.-Y., An efficient immersed boundary-lattice Boltzmann method for the hydrodynamic interaction of elastic filaments, *Journal of Computational Physics*, Vol. 230, 2011, pp. 7266-7283.

[9] Favier J., Revell A. and Pinelli A., A Lattice Boltzmann-Immersed Boundary method to simulate the fluid interaction with moving and slender flexible objects, *Journal of Computational Physics*, Vol. 261, 2014, pp. 145-161.

[10] De Rosis A., Falcucci G., Ubertini S. and Ubertini F., Aeroelastic study of flexible flapping wings by a coupled lattice Boltzmann-finite element approach with immersed boundary method, *Journal of Fluids and Structures*, Vol. 49, 2014, pp. 516-533.

[11] Gilmanov A. & Acharya S., A hybrid immersed boundary and material point method for simulating 3D fluid-structure interaction problems, *Int. J. Numer. Meth. Fluids*, Vol. 56, 2008, pp. 2151-2177.

[12] Wang Z., Fan J., and Luo K., Combined multi-direct forcing and immersed boundary method for simulating flows with moving particles, *International Journal of Multiphase Flow*, Vol. 34, 2008, pp. 283-302.

[13] Suzuki K. & Inamuro T., Effect of internal mass in the simulation of a moving body by the immersed boundary method, *Computers and Fluids*, Vol. 49, 2011, pp. 173-187.

[14] Huang W.-X. & Sung H.J., An immersed boundary method for fluid flexible structure interaction, *Computer Methods in Applied Mechanics and Engineering*, Vol. 198, 2009, pp. 2650-2661.

[15] Huang W.-X. & Sung H.J., Three-dimensional simulation of a flapping flag in a uniform flow, *Journal of Fluid Mechanics*, Vol. 653, 2010, pp. 301-336.